Molecular disturbance underlies to arrhythmogenic cardiomyopathy induced by transgene content, age and exercise in a truncated PKP2 mouse model

Javier Moncayo-Arlandi,[1,2] Eduard Guasch,[3] Maria Sanz,[4] Marta Casado,[5] Nahuel Aquiles García,[6] Lluis Mont,[3] Marta Sitges,[4] Ralph Knöll,[7] Byambajav Buyandelger,[7] Campuzano Oscar[1,9], Antonio Diez-Juan,[8]*[†] Ramon Brugada,[1,9,10]*[†] FACC, FESC.

[1]Cardiovascular Genetic Centre, Institute of Biomedical Research of Girona (IDIBGI), Girona, Spain; [2]Department of Biochemistry and Molecular Biology, University of Valencia, Valencia, Spain; [3]Arrhythmia Unit, Cardiology Department, Hospital Clínic, Universitat de Barcelona and IDIBAPS, Barcelona, Catalonia, Spain; [4]Imaging Section, Cardiology Department, Hospital Clínic, Universitat de Barcelona and IDIBAPS, Barcelona, Catalonia, Spain; [5]Institute of Biomedicine of Valencia, IBV-CSIC, Valencia, Spain; [6]Mixed unit for Cardiovascular Repair, Instituto de Investigación Sanitaria La Fe-Centro de Investigación Príncipe Felipe, Valencia, Spain; [7]Department of Medicine, Integrated Cardio Metabolic Centre (ICMC), Karolinska Institutet, Huddinge, Sweden;[8]Fundación IVI/INCLIVA and IGENOMIX, Valencia, Spain;[9]Medical Science Department, School of Medicine, University of Girona and[10]Cardiovascular Genetics Clinic, Hospital Josep Trueta, Girona, Spain.

†Equal contribution

*Co-Corresponding authors:

Ramon Brugada: Cardiovascular Genetic Centre, Institut d´Investigació Biomèdica de Girona Dr. Trueta-IDIBGI, Edifici M2, Parc Hospitalari Martí I Julià, 17190 Salt, Spain. Tel: (+34)872-987-087. Fax 972 485422. Email: rbrugada@idibgi.org

Antonio Diez-Juan: IGENOMIX, Valencia, Spain. Email: antonio.diez@igenomix.com.

2

Abstract

Arrhythmogenic cardiomyopathy (ACM) is a disorder characterized by a progressive ventricular myocardial replacement by fat and fibrosis which lead to ventricular arrhythmias and sudden cardiac death. Mutations in the desmosomal gene Plakophilin-2 (PKP2) accounts for >40% of all known mutations, generally causing a truncated protein. In a PKP2 truncated mouse model, we hypothesize that content of transgene, endurance training and aging will be determinant in disease progression. In addition, we investigated the molecular defects associated with the phenotype in this model. We developed a transgenic mouse model containing a truncated PKP2 (PKP2-Ser329) and generated three transgenic lines expressing increasing transgene content. The pathophysiological features of ACM in this model were assessed. While we did not observe fibro-fatty replacement, ultrastructural defects were exhibited. Moreover, we observed transgene content-dependent development of structural (ventricle dilatation and dysfunction) and electrophysiological anomalies in mice (PR interval and QRS prolongation and arrhythmia induction). In concordance with pathological defects, we detected a content reduction and remodeling of the structural proteins Desmocollin-2, Plakoglobin, native Plakophilin-2, Desmin and β-Catenin as well as the electrical coupling proteins Connexin 43 and cardiac sodium channel ($Na_v1.5$). Surprisingly, we observed structural but not electrophysiological abnormalities only in trained and old mice. We demonstrated that truncated PKP2 provokes ACM in absence of fibro-fatty replacement in the mouse. Transgene dose is essential to reveal the pathology, whereas aging and endurance training trigger limited phenotype. Molecular abnormalities underlay the structural and electrophysiological defects.

Introduction

The arrhythmogenic cardiomyopathy (ACM) is a cardiac disease characterized by a progressive fibro-fatty tissue replacement, predominant right ventricle dilatation and dysfunction, and ventricular arrhythmias. ACM is an important cause of sudden cardiac death,(1) particularly among athletes. In ACM patients, sudden death is 5-fold higher in athletes than in sedentary patients,(2) underscoring the role of exercise as a trigger for ventricular arrhythmias.

ACM is a familial disease in ~50% of patients. Mutations in desmosomal proteins Desmocollin-2 (DSC2), Desmoglein-2 (DSG2), Plakophilin-2 (PKP2), Plakoglobin (PG) and Desmoplakin (DSP) have been associated with ACM. More than 40% of mutations affect PKP2, usually frameshift mutations leading to truncated PKP2 proteins.(3)

PKP2 regulates desmosome assembly and contributes to its mechanical strength,(4) evolving as an essential component in cardiac morphogenesis and wall integrity.(5) PKP2 accumulates in the intercalated discs of cardiomyocytes (ID), which harbor proteins such as Connexin43 (CX43; from GAP junctions) or the cardiac sodium channel (Na$_v$1.5).(6-8) The absence of PKP2 expression yields remarkable electrical effects, highlighting its critical contribution to cardiac electrical properties. Indeed, a haploinsufficient PKP2 mouse model shows slow conduction velocity, sodium current deficit and ventricular arrhythmias.(9)

Truncated PKP2 forms interact with structural and electrical proteins *in vitro*,(7, 10) potentially contributing to ACM pathogenesis. Despite the importance of PKP2-truncated mutations in ACM epidemiology, little is known on their pathological and molecular features. We therefore developed a transgenic mouse model carrying a

truncated PKP2 expressing the first 329 amino acids versus 881 amino acids of the full protein. We investigated whether the addition of an increasing content of a truncated PKP2 protein is able to promote structural and electrical ACM abnormalities and assessed possible molecular mechanisms. Finally, we studied the effects of well-known contributors to ACM progression: aging and exercise.

Results

Five transgenic lines were obtained after transgenesis. The molecular and immunofluorescence analysis confirmed the transgene expression in heart (Figure 1B and Supplementary Figure 1). In addition, the transcript expression in liver was almost undetectable (Figure 1C), thus indicating cardiac tissue-specific expression (n=3 per group). In the heart, lines 4 (L4) and 5 (L5) presented with the highest transcript amount, with expression in L4 roughly doubling L5. These findings were confirmed at the protein level (Figure 1D). Thus, L4 and L5 were selected for further analyses. In order to increase the transgene content, a L4+L5 heterozygous transgenic line was created (see Methods, Supplementary Methods and Supplementary Figure 2).

Overall, the protein analysis revealed a gradient of transgene expression over the 3 transgenic lines: line 5 (low expression: TG-L), line 4 (medium expression: TG-M) and line 4+5 (high expression: TG-H) (Figure 1E). We obtained similar numbers of transgenic (TG) and wild type (WT) animals in each littermate. In addition, we did not find any increment of mortality in adult mice of any transgenic group.

Native and truncated PKP2 localization and distribution in cardiomyocytes

Truncated PKP2 proteins might compete with the binding sites of the full PKP2 protein.(11) We therefore investigated the localization and distribution of endogenous,

native PKP2 protein and truncated PKP2 within the cardiomyocyte of 7 months-old mice. Both native PKP2 and truncated PKP2 co-localized in the ID of the cardiomyocytes of transgenic mice (Figure 2A). However, truncated PKP2 was also observed in the cytoplasm of transgenic cardiomyocytes and some nuclei of transgenic cardiomyocytes contained truncated PKP2 (Figure 2A).

We next analyzed the relative content of native and truncated PKP2 in different subcellular compartments (Figure 2B). As expected, native PKP2 amount was undetectable in cytosolic and nuclear protein sub-fraction and accumulated in the membrane and cytoskeleton compartments. In contrast, truncated PKP2 was distributed in the nucleus, cytosol, membrane and particularly, in cytoskeleton compartments (Figure 2B).

Truncated PKP2 induces ultrastructural defects without fibro-fatty replacement in mouse

We used 10 month-old mice from WT, TG-L, TG-M and TG-H lines for histological analysis (n≥10 animals per group). Cardiomyocyte morphology was similar in all groups and no evident collagen deposition or fatty tissue replacement was found in TG-L, TG-M or TG-H hearts (Supplementary Figure 3A). In addition, the presence of truncated PKP2 did not result in a significant cardiac hypertrophy (Supplementary Figure 3B).

Ultrastructural evaluation revealed defects in the ID and desmosome integrity in TG-H hearts (n=3 per group; Figures 3 and 4). ID structure was similar in TG-M and WT mice (Figure 3). In contrast, loss of cell-to-cell adhesion were observed in TG-H (Figure 3C), and complete IDs ruptures were frequent (Figure 3D; Supplementary Figure 4). The quantitative analysis of the distance between cardiomyocytes at ID level

showed significant detachment in TG-H compared with TG-M and WT mice (Figure 3G). Moreover, desmosomal disassembly, a decrease of face-to-face contact and no recognizable layers were observed in TG-H hearts (Figure 4C).

Structural and hemodynamic changes are driven by truncated PKP2 content and adhesion proteins defects

Echocardiographic studies in 7 month-old sedentary mice showed no changes in LV structure and function in TG-L and TG-M mice in comparison to WT (Table 1). However, a profound reduction in LV systolic function was found in TG-H mice as demonstrated by a decreased LVFS (Table 1). Conversely, evident changes were found in the RV function and structure in TG-H mice and, to a lesser extent, in TG-L and TG-M groups (Table 1). The RVOT was significantly dilated in TG-H, whereas no significant dilatation was found in TG-L or TG-M mice (Figure 5). Mild RV dilation was also found in TG-L and TG-M at the chamber level. RV systolic dysfunction was only evident in the animals with the highest transgene content, likely leading to a decreased ability to raise pulmonary pressure (Table 1).

To study the molecular mechanisms of structural alterations in transgenic hearts we assessed the localization of several adhesion proteins. All adhesion proteins were present in the ID of all groups. Nevertheless, β-CAT presence was progressive switched from the ID region to the cytoplasm over transgene content in TG-M and -H cardiomyocytes (open arrows and asterisk in Figure 6A; Supplementary Figure 6). In addition, abnormal deposits of DSC2 were also evident in the cytoplasm of some cardiomyocytes in the TG-H line, but not in TG-M or WT animals (Figure 6B and Supplementary Figure 6). There was no delocalization of PG and DSP in any group

(Supplementary Figure 5 and 6). All changes were similarly observed in the RV, LV and IVS.

The total amount of structural proteins was then quantified by mean of western-blotting (Figure 6C and D). No differences were found between WT and TG-M in any of the proteins tested. However, a significant decrease in protein amount was noted in TG-H for native PKP2, PG, DES and β-CAT (Figure 6D).

Truncated PKP2 prompts a dose-dependent ventricular arrhythmia susceptibility and CX43 and Na$_v$1.5 remodeling and reduction

Main ECG findings are presented in the Figure 7, and analyses summarized in the Supplementary Table. Representative ECGs from WT, TG-M and TG-H of sedentary 7-month mice show a progressive PR interval prolongation over TG load (Figure 7A and upper graph in Figure 7B). QRS was prolonged only in the TG-H group (lower graph in Figure 7B). No differences in heart rate, P-wave or QTc duration were found in any group (Supplementary Table). Atrio-ventricular conduction assessment showed a progressive prolongation of Atrial-His conduction (A-H interval) with the content of transgene (Table 2), similar to the PR-interval findings.

Susceptibility to ventricular arrhythmias was tested by mean of electrical programmed stimulation (Figure 8). Ventricular tachycardia was induced in 31% of WT mice; inducibility progressively increased with transgene content, and was remarkably more frequent in the TG-H group (74% of tested mice) (Figure 8), thus confirming a transgene dose-dependent increase in ventricular arrhythmia susceptibility (p=0.01).

We investigated changes in proteins involved in electrical coupling potentially contributing to electrical disturbances in our model. Both the distribution and content of CX43 and Na$_v$1.5 were studied (Figure 9 and Supplementary Figure 7). CX43 plays a

crucial role in electrical intercellular communication. The distribution of CX43 in the ID of cardiomyocytes was similar in WT and TG-M groups. Nonetheless, CX43 distributed in a wider, blurrier way in the ID of the RV, LV and IVS of TG-H mice (Figure 9A and Supplementary Figure 7), consistent with desmosome disarrangement (Figure 4). Protein quantification demonstrated a significant, progressive reduction of CX43 from WT to TG-H (Figure 9C).

Fast sodium current generates the upstroke phase of the action potential and modulates conduction velocity throughout myocardium. We observed a reduced $Na_v1.5$ localization in the ID of the RV, LV and IVS of TG-H and, to a lesser extent, TG-M mice (Figure 9B and Supplementary Figure 7). Western-blot quantification showed a mild reduction in TG-M but a dramatic reduction (~60%) in TG-H mice in comparison to WT (Figure 9D).

Aging and exercise unmask structural, but not electrical features, in the mouse model

The effects of aging and endurance training, two prominent physiological insults in ACM, were studied in our animal model. Physical activity is a prominent contributor to ACM progression in patients with a predisposing mutation.(12) We therefore aimed at unmasking an overt ACM phenotype in TG-L and TG-M mice by mean of long-term physical activity; trained WT mice served as controls. All trained groups developed significant cardiac hypertrophy in comparison to sedentary mice, but heart/body weight ratio remained similar in trained WT and TG groups (Supplementary Figure 3D). No evident fatty tissue replacement or inflammatory infiltrates were observed in trained WT or TG mice (WT: n=5; TG-L: n=5; TG-M: n=6). However, physical exercise promoted RVOT dilation in TG-M and TG-L mice, thus unmasking structural ACM abnormalities (Figure 5). Exercise training prompted QRS prolongation in all groups

9

but did not unmask further differences between transgenic and WT animals (Figure 7B). Physical activity did increase arrhythmia inducibility in WT mice in comparison to sedentary animals, but no inducibility differences were found between sedentary and trained transgenic groups (Figure 8).

The natural progression of ACM was assessed at different ages. Structural RV remodeling progressed with time: in contrast to 7-month mice, aged (12 month-old) TG-L and TG-M mice showed RVOT, RV diameter and RV area dilation in comparison to WT (Figure 5 and Table 1). This was accompanied by RV dysfunction in all aged transgenic mice. Nevertheless, neither the PR interval nor QRS complex prolongation were affected by age (PR Interval, p=0.85; QRS duration, p=0.22) (Figure 7B).

Discussion

Plakophilin-2 is a desmosomal protein that maintains mechanical adhesion between cardiomyocytes and supports the mechanical stress developed during cardiac contractions. Recent data have described an interaction of PKP2 with CX43 and $Na_v1.5$ channels. It has been described that PKP2 provides structural support of such proteins in the membrane, facilitating their function during the cardiac action potential(7). This fact suggests that PKP2 has an important role in structural as well as electrical properties in the heart. Interestingly, PKP2 is an important gene in the pathology of ACM. Multiple truncated variants of this protein have been associated to ACM patients, yielding a high variability of expressivity and penetrance. This variability suggests that environmental factors, in addition to genetically-determined ones, could play an important role in ACM pathogenesis(13).

We therefore, inspected the pathophysiological consequences of a truncated PKP2 in a new animal model, and explored potential molecular contributors to this

10

phenotype. In addition, we investigated the effect of two environmental factors related to ACM progression: endurance training and aging.

Myocardial fibro-fatty replacement is a hallmark of ACM patients that is often considered an essential process in its pathogenesis. We therefore characterized the myocardial tissue of all transgenic lines; the trained group was also examined upon a potential role of exercise as a trigger for fibro-fatty replacement. However, we did not observe any evident tissue replacement in any group. This phenotype is in concordance with a mild phenotype observed in TG-L and -M and contrasts with models presenting with tissue replacement, an accelerated ACM progression and an increased mortality(14, 15). However, fibro-fatty replacement was also absent in TG-H mice in our model, a transgenic line showing a highly expressive structural, ECG and arrhythmic phenotype, similar to other models presenting with tissue replacement. This fact indicates that fibro-fatty tissue development is not induced in this model. The fibro-fatty tissue formation depends on the suppression of Wnt/β-cat pathway,(16) a process which could be interfered in this model. It has been recently demonstrated that PKP2 knock-out suppresses the Wnt/β-cat pathway.(17) On the other hand, the PKP2 overexpression reduces the lipid accumulation in ACM patients-derived cells; truncated PKP2 accumulation in cardiomyocyte nuclei in our model (Figure 2) might prevent the differentiation towards an adipocyte-like fate. In addition, β-CAT remodeling promoted by truncated PKP2 (Figure 6 and Supplementary Figure 6) could further interfere with this process by modifying the normal amount of β-CAT in the nucleus, eventually resulting in the absence of fibro-fatty tissue. Although more mechanistic studies are warranted, our findings demonstrate that fibro-fatty replacement is not necessary to trigger an ACM phenotype, consistent with previous models.(18, 19)

11

The transgene content is a clear determinant of the disease severity in our model. Particularly, RV enlargement (measured by RVOT) and electrical abnormalities (PR interval duration and arrhythmias inducibility) were associated with truncated PKP2 amount in each of the transgenic lines. Recently, *in vitro* studies showed that truncated PKP2 in ACM patients are associated with a lower expression of PKP2, suggesting that PKP2 haploinsufficiency contributes to its pathogenesis(11). Indeed, the profound phenotype observed in TG-H mice in our model could be interpreted as the result of reduced content of native PKP2 in this line (Figure 6). Nevertheless, TG-M shows some features of ACM, mostly electrophysiological ones, in the absence of native PKP2 reduction, which may be explained by a dominant negative effect of truncated PKP2 in the cardiac tissue, as previously described for other mutations in ACM patients(20). Overall, our results indicate that balance between mutated and native PKP2 eventually determine the ACM phenotype. In addition to the balance of native/mutated PKP2 and environmental factors, the disease penetrance and expressivity could also be determined by compound and digenic heterozygosity. A frequency of two different desmosomal mutations in the same patient (~16% of genotyped patients),(21, 22) suggests that this fact confers a major predisposition to ACM development. Furthermore, such carriers show a higher disease expressivity compared with single-mutation patients.(23) Therefore, other genetics factors as the combination with another desmosomal mutation could generate the full expression of ACM phenotype in our animal model.

Several factors modulate ACM progression in addition to truncated PKP2 content. Both age and regular physical activity have been linked to ACM progression in patients.(1, 2) Here, we confirmed that endurance training and aging trigger RV enlargement in transgenic animals. Strikingly, neither physical activity nor aging enhanced the ECG abnormalities or arrhythmia inducibility in transgenic mice. The

reasons for the lack of changes in electrical properties remain unclear. It is possible that the training protocol was not intense enough to trigger electrical abnormalities in our model. However, we observed prolonged QRS and an increase of arrhythmia inducibility in WT trained mice, demonstrating exercise-promoted remodeling, consistent with previous animal models(24) and clinical studies.(25) In this sense, a swimming protocol might reveal electrical defects, in concordance with other ACM mouse models.(18, 26) Nonetheless, our protocol extended over a long period (24 weeks) compared to common swimming protocols used in other studies (7-8 weeks).(18, 19) On the other hand, we detected structural, but not electrical defects related to aging. The study in old mice could not reveal a prolonged QRS, although similar ACM mouse models showed this electrical defect in younger animals (10 months-old).(26) Altogether, these data suggest that structural remodeling is subject to genetic but also to environmental factors, while primary electrical disturbances do only depend on transgene amount in this model.

The genetic association of desmosomal genes with ACM suggests that disturbance of proteins and desmosomes disassembly underlay its pathogenesis. In fact, this model showed ruptures of intercalated discs and desmosomes, demonstrating the reduction of adhesion between cardiomyocytes in presence of truncated PKP2. In concordance with this result, we observed a decrease and remodeling of some adhesion proteins, which could explain such effects. Molecular and ultra-structural anomalies were only observed in the TG-H line, suggesting that amount of transgene was essential to reveal this phenotype.

PKP2 interacts with different channels in the cardiac tissue, stabilizing them in the membrane. Besides, its deficiency results in a reduction of sodium current, slower conduction velocity and arrhythmogenesis.(9) Likewise, our model also developed

some electrophysiological abnormalities. In order to identify the molecular determinants of this phenotype, we investigated two channels that interact with PKP2 in the cardiac tissue: CX43(8) and Na$_v$1.5.(7) We observed a dramatically reduction and remodeling of both proteins associated to electrical anomalies in this model. Interestingly, only the N´terminal domain of PKP2 is required to bind Na$_v$1.5(7) and CX43.(10) The truncated PKP2 protein in this model exclusively expresses the N'terminal domain, likely retaining its ability to bind Na$_v$1.5 and CX43. Altogether, these data suggest the importance of PKP2 in the stabilization of these channels in the membrane of the cardiomyocytes.

In contrast to western blot quantification, we did not observe a reduction of signal intensity in TG-H mice for some of the proteins analyzed by immunofluorescence studies. However, immunofluorescence technique presents many limitations. Several factors such as antibodies dilution, section orientation and tissue shrinkage can bias the results. Some ACM studies have demonstrated a poor correlation between immunofluorescence signal and western blot quantification, suggesting that immunofluorescence should be considered a qualitative, rather than a quantitative, technique.(26, 27)

Mutations in a single gene may drive to a variety of different pathologies.(28) For example, mutations in DSP, classically associated with ACM, have been also reported in idiopathic dilated cardiomyopathy (DCM)(29) patients, showing an overlap of genes responsible for different cardiomyopathies.(28) Even the same mutation might be associated with different diseases. The R14del mutation in Phospholamban protein provokes ACM as well as DCM,(30) suggesting a close relationship between both diseases likely influenced by the environmental and genetic background. Our findings suggest that the amount of truncated PKP2 critically determines different clinical

entities, from predominant RV involvement to ECG abnormalities or LV involvement. These entities are further modulated by physiological factors such as aging and regular physical activity. Mutations in PKP2 have been associated with ACM, but also DCM(31) and Brugada syndrome (BrS).(32) In addition, ACM patients carrying missense PKP2 mutations are able to show Brugada-like ECG,(33) while some BrS patients present with PR interval and QRS prolongation and RVOT dilatation,(34) similar to findings in our animal model. Thus, this model allows us to speculate on blurried limits established between ACM, BrS and DCM from clinical practice.

In summary, we present a new truncated PKP2 mouse model which develops some ACM features in absence of fibro-fatty tissue. The transgene content determines the severity of these characteristics, whereas aging and endurance training unmasked the structural, but not electrophysiological phenotype in this model. Furthermore, molecular disturbances underlay to structural and electrophysiological anomalies. This work provides new molecular and physiological insights into the development and progression of ACM causing by a truncated PKP2 protein. Finally, these data suggest that, at least in part, the strategies focused in reducing amount/expression of mutated PKP2 could have a positive effect in ACM future treatments.

Limitations

Some limitations of our work should be acknowledged. In contrast to patients, this model presents two fully normal copies of PKP2 to which a truncated protein has been added, likely reducing the pathogenic effect of a mutated PKP2. However, with this approach we could test and isolate the pathogenic role of a mutated PKP2, ruling out the contribution of haploinsufficiency. Western blots analyses were performed only with ventricular tissue homogenized from both ventricles which could have diluted a

different effect in the RV and LV. Nevertheless, immunofluorescence studies allowed differential analyses from the RV, LV and IVS. Finally, our findings might not be applicable to all ARVC-causing mutations, and further studies with other mice models carrying distinct truncated PKP2 would allow us to compare both phenotypes.

Materials and Methods

Refer to the Supplementary Methods for a detailed description of the methodology used in this work.

Construct design and transgenic mice generation

A DNA construct containing an α-myosin heavy chain (α-MHC) promoter upstream to a truncated PKP2 sequence (codifying the first 329aa versus 837aa of the full protein) fused to the tags T2a and Ruby (Figure 1A) was introduced into B6D2F1 mouse embryos by conventional methods. Successful insertion into genomic DNA was checked with polymerase chain reaction (PCR) and primers specifically targeting the truncated PKP2 sequence. We confirmed the transgene expression by transcript and protein presence, which showed a successful T2a-peptide cardiac auto-cleavage (Supplementary Figure 1). Ten different transgenic mice were obtained; males were selected as founders of each transgenic line (n=5).

A transgenic line with a higher transgene expression was obtained after two sequential generations of both L4 and L5 heterozygous lines (Supplementary Figure 2A). Eventually, a heterozygous line including one L4 copy and one L5 copy was obtained. Real time quantitative PCR (qPCR) demonstrated higher genomic transgene content in this line (Supplementary Figure 2B and 2C).

16

The animals were housed in standard environment conditions and fed regular chow and water *ad libitum*. The animals were handled in accordance with the Spanish Regulations for the protection of Experimental Animals (R.D. 1201/2005) and the guidelines of the European Parliament on the protection of animals used for scientific purposes (Directive 2010/63/EC). All procedures were approved by the institutional animal research ethics committees.

Training protocol

3-month old mice were undergone to endurance training in a treadmill (Panlab; LE8710M) for 1 hour/day, 5 days/week for 16 weeks. The maximum treadmill speed was progressively increased from 30cm/s to 45cm/s during the 16-week training. An electrical shock (0.18-0.4mA) at the back of the treadmill was used to condition animals to run; animals not running properly were excluded.

Electrocardiogram and electrophysiological studies

All *in vivo* procedures were carried out in anesthetized mice (1.5% inhaled isoflurane) at a body constant temperature (37.0±0.3°C). A DII-lead baseline electrocardiogram (ECG) was obtained in all animals, and P-wave, PR-interval, QRS duration and Bazett-corrected QT (QTc) interval duration were measured.

Electrophysiological studies were carried out as previously described, with minor modifications.(30) Briefly, an octopolar EP catheter (Scisense, London, ON, Canada) was introduced in the right jugular vein and carefully advanced into the right ventricle. A His electrogram (EGM) was recorded and the A-H and H-V intervals were measured. The ventricular refractory period was assessed with a 9-pulse train (S1=100 ms) followed by an S2 which was progressively shortened in 1-ms steps up to loss of ventricular capture. The ventricular refractory period was defined as the shortest S2-

17

coupling interval inducing a ventricular beat. Ventricular arrhythmia inducibility was tested by mean of two and three extrastimuli after a 9-pulse train (S1=100ms and 80ms) and burst-pacing techniques. Ventricular tachycardia (VT) was defined as 3 or more consecutive ventricular beats after the last pacing spike. Only reproducible ventricular tachycardias were considered.

Echocardiography

Transthoracic echocardiographic studies were carried out >6 hours after the last training session under general anesthesia (1.5% inhaled isoflurane) with a 10S (11.5 Megahertz) phased array probe in a Vivid Q instrument (GE Medical, Milwaukee, USA). The short parasternal (SAx) and long parasternal (LAx) axis views were used to assess LV and RV size, respectively. RV systolic function was assessed by tricuspid annular plane systolic excursion (TAPSE) in a 4-chamber view. LV systolic function was assessed by endocardial fractional shortening (LVFS).

RNA extraction and Real time qPCR

Total RNA was extracted from cardiac and liver tissue. Transcript amount of truncated *Pkp2*, native *Pkp2* and glyceraldehyde-3-phosphate-dehydrogenase (*Gapdh*) quantified by mean of real-time qPCR with a KAPA SYBR FAST qPCR kit. Results are shown with the $2^{-\Delta\Delta Ct}$ method. *Gapdh* was used as housekeeping.

Western blot and compartmentalized protein extraction

Total protein from ventricles of 7 month-old mice was extracted and used for western blot analysis of the following proteins: T2a tag, PKP2, CX43, DSC2, PG, DSP, $Na_v1.5$, GADPH, α-MHC, β-catenin (β-CAT), Desmin (DES), Histone H3-tri methyl K9 (H3K9), and Sodium/Potassium ATPase. Densitometry analysis was performed with

18

ImageJ software (NIH, Bethesda, USA). To localize truncated and native PKP2 forms, nuclear, cytosolic and membrane proteins sub-fractions were isolated using a commercial kit (Millipore; cat #2145).

Histology and immunofluorescence

Masson´s trichrome staining was performed in ventricular paraffin-embedded sections for a general cardiac tissue overview. Picrosirius red stain was used to assess collagen fibers. Oil-O-red staining (for fatty tissue infiltration assessment) and immunofluorescence were performed in cryosections. Immunofluorescence experiments targeted the following proteins: T2a tag, PKP2, CX43, DCS2, PG, DSP, DES, β-CAT and $Na_v1.5$. Microphotographs were obtained using an A1R confocal microscope (Nikon).

Transmission electron microscopy

Hearts were perfused with fixative solution (2% PFA and 2.5% Glutaraldehyde in sodium cacodylate 0.1M), cut in 1-1.5mm^3 pieces and post-fixed during 4h. Then, they were included in epoxy resin and 60nm ultrathin sections were scanned in a transmission electron microscope (Zeiss DSM, Oberkochen, Germany).

Statistical analysis

All data are shown as mean±SEM. Analyses were performed using unpaired *t*-test when two groups were compared; one way-ANOVA and Bonferroni post-test when transgenic lines and WT were compared (3/4 groups), and two way-ANOVA and Bonferroni post-test when transgenic lines were combined with age/training conditions (2 main factors). Non parametric Kruskal-Wallis method and posterior Dunnet post-test was used in not-normally distributed variables. Mantel-Haenszel linear-by-linear

Association was performed to test the trend between categorical variables. Statistical analyses were performed using SPSS v19.0 (IBM) and GraphPad Prism Software v5.03.

Acknowledgments

Statement

None declared.

Conflict of interest

None declared.

References

1. Thiene G, Corrado D, Basso C. (2007) Arrhythmogenic right ventricular cardiomyopathy/dysplasia. *Orphanet J. Rare Dis.*, **2**, 45.

2. Corrado D, Basso C, Rizzoli G, Schiavon M, Thiene G. (2003) Does sports activity enhance the risk of sudden death in adolescents and young adults?. *J. Am. Coll. Cardiol.*, **42**,1959-1963.

3. Awad MM, Calkins H, Judge DP (2008) Mechanisms of disease: molecular genetics of arrhythmogenic right ventricular dysplasia/cardiomyopathy. *Nat. Clin. Pract. Cardiovasc. Med.*, **5**, 258-267.

4.   Bass-Zubek AE, Godsel LM, Delmar M, Green KJ (2009) Plakophilins: multifunctional scaffolds for adhesion and signaling. *Curr. Opin. Cell. Biol.*, **21**, 708-716.

5.   Grossmann KS, Grund C, Huelsken J, Behrend M, Erdmann B, Franke WW, Birchmeier W (2004) Requirement of plakophilin 2 for heart morphogenesis and cardiac junction formation. *J. Cell. Biol.*, **167**, 149-160.

6.   Oxford EM, Musa H, Maass K, Coombs W, Taffet SM, Delmar M (2007) Connexin43 remodeling caused by inhibition of plakophilin-2 expression in cardiac cells. *Circ. Res.*, **101**,, 703-711.

7.   Sato PY, Musa H, Coombs W, Guerrero-Serna G, Patiño GA, Taffet SM, Isom LL, Delmar M (2009) Loss of plakophilin-2 expression leads to decreased sodium current and slower conduction velocity in cultured cardiac myocytes. *Circ. Res.*, **105**,523-526.

8.   Sato PY, Coombs W, Lin X, Nekrasova O, Green KJ, Isom LL, Taffet SM, Delmar M(2011) Interactions between ankyrin-G, Plakophilin-2, and Connexin43 at the cardiac intercalated disc. *Circ. Res.*, **109**,193-201.

9.   Cerrone M, Noorman M, Lin X, Chkourko H, Liang FX, van der Nagel R, Hund T, Birchmeier W, Mohler P, van Veen TA et al. (2012) Sodium current deficit and arrhythmogenesis in a murine model of plakophilin-2 haploinsufficiency. *Cardiovasc. Res.*, **95**,460-468.

10.   Joshi-Mukherjee R, Coombs W, Musa H, Oxford E, Taffet S, Delmar M (2008) Characterization of the molecular phenotype of two arrhythmogenic right ventricular

cardiomyopathy (ARVC)-related plakophilin-2 (PKP2) mutations. *Heart Rhythm.*, **5**, 1715-1723.

11.   Rasmussen TB, Nissen PH, Palmfeldt J, Gehmlich K, Dalager S, Jensen UB, Kim WY, Heickendorff L, Mølgaard H, Jensen HK, et al. (2014) Truncating Plakophilin-2 Mutations in Arrhythmogenic Cardiomyopathy Are Associated With Protein Haploinsufficiency in Both Myocardium and Epidermis. *Circ. Cardiovasc. Genet.*, **7**, 230-240.

12.   Ruwald AC, Marcus F, Estes NA, 3rd, Link M, McNitt S, Polonsky B, Calkins H, Towbin JA, Moss AJ, Zareba W (2015) . Association of competitive and recreational sport participation with cardiac events in patients with arrhythmogenic right ventricular cardiomyopathy: results from the North American multidisciplinary study of arrhythmogenic right ventricular cardiomyopathy. *Eur. Heart J.*, **36**, 1735-1743.

13.   Sawant AC, Bhonsale A, te Riele AS, Tichnell C, Murray B, Russell SD, Tandri H, Tedford RJ, Judge DP, Calkins H (2014) Exercise has a disproportionate role in the pathogenesis of arrhythmogenic right ventricular dysplasia/cardiomyopathy in patients without desmosomal mutations. *J. Am. Heart Assoc.*, **3**, e001471.

14.   Lyon RC, Mezzano V, Wright AT, Pfeiffer E, Chuang J, Banares K, Castaneda A, Ouyang K, Cui L, Contu R, et al. (2014) Connexin defects underlie arrhythmogenic right ventricular cardiomyopathy in a novel mouse model. *Hum. Mol. Genet.*, **23**, 1134-1150.

15.   Pilichou K, Remme CA, Basso C, Campian ME, Rizzo S, Barnett P, Scicluna BP, Bauce B, van den Hoff MJ, de Bakker JM, et al. (2009) Myocyte necrosis underlies progressive myocardial dystrophy in mouse dsg2-related arrhythmogenic right ventricular cardiomyopathy. *J. Exp. Med.*, **206**, 1787-1802.

16.   Garcia-Gras E, Lombardi R, Giocondo MJ, Willerson JT, Schneider MD, Khoury DS, Marian AJ (2006) Suppression of canonical Wnt/beta-catenin signaling by nuclear plakoglobin recapitulates phenotype of arrhythmogenic right ventricular cardiomyopathy. *J. Clin. Invest.*, **116**, 2012-2021.

17.   Chen SN, Gurha P, Lombardi R, Ruggiero A, Willerson JT, Marian AJ (2014) The hippo pathway is activated and is a causal mechanism for adipogenesis in arrhythmogenic cardiomyopathy. *Circ. Res.*, **114**, 454-468.

18.   Cruz FM, Sanz-Rosa D, Roche-Molina M, García-Prieto J, García-Ruiz JM, Pizarro G, Jiménez-Borreguero LJ, Torres M, Bernad A, Ruíz-Cabello J, et al. (2015) Exercise triggers ARVC phenotype in mice expressing a disease-causing mutated version of human plakophilin-2. *J. Am. Coll. Cardiol.*, **65**, 1438-1450.

19.   Kirchhof P, Fabritz L, Zwiener M, Witt H, Schäfers M, Zellerhoff S, Paul M, Athai T, Hiller KH, Baba HA, et al. (2006) Age- and training-dependent development of arrhythmogenic right ventricular cardiomyopathy in heterozygous plakoglobin-deficient mice. *Circulation.*, **114**, 1799-1806.

20.   Rasmussen TB, Palmfeldt J, Nissen PH, Magnoni R, Dalager S, Jensen UB, Kim WY, Heickendorff L, Mølgaard H, Jensen HK, et al. (2013) Mutated desmoglein-2 proteins are incorporated into desmosomes and exhibit dominant-negative effects in arrhythmogenic right ventricular cardiomyopathy. *Hum. Mut.*, **34**, 697-705.

21.   Rigato I, Bauce B, Rampazzo A, Zorzi A, Pilichou K, Mazzotti E, Migliore F, Marra MP, Lorenzon A, De Bortoli M, et al. (2013) Compound and digenic heterozygosity predicts lifetime arrhythmic outcome and sudden cardiac death in desmosomal gene-related arrhythmogenic right ventricular cardiomyopathy. *Circ. Cardiovasc. Genet.*, **6**, 533-542.

22.   Xu T, Yang Z, Vatta M, Rampazzo A, Beffagna G, Pilichou K, Scherer SE, Saffitz J, Kravitz J, Zareba W, et al. (2010) Compound and digenic heterozygosity contributes to arrhythmogenic right ventricular cardiomyopathy. *J. Am. Coll. Cardiol.*, **55**, 587-597.

23.   Bauce B, Nava A, Beffagna G, Basso C, Lorenzon A, Smaniotto G, De Bortoli M, Rigato I, Mazzotti E, Steriotis A, et al. (2010) Multiple mutations in desmosomal proteins encoding genes in arrhythmogenic right ventricular cardiomyopathy/dysplasia. *Heart Rhythm.*, **7**, 22-29.

24.   Benito B, Gay-Jordi G, Serrano-Mollar A, Guasch E, Shi Y, Tardif JC, Brugada J, Nattel S, Mont L (2011) Cardiac arrhythmogenic remodeling in a rat model of long-term intensive exercise training. *Circulation.*, **123**, 13-22.

25.   van Tintelen JP, Entius MM, Bhuiyan ZA, Jongbloed R, Wiesfeld AC, Wilde AA, van der Smagt J, Boven LG, Mannens MM, van Langen IM, et al. (2006) Plakophilin-2 mutations are the major determinant of familial arrhythmogenic right ventricular dysplasia/cardiomyopathy. *Circulation.*, **113**, 1650-1658.

26.   Fabritz L, Hoogendijk MG, Scicluna BP, van Amersfoorth SC, Fortmueller L, Wolf S, Laakmann S, Kreienkamp N, Piccini I, Breithardt G, (2011) et al. Load-reducing therapy prevents development of arrhythmogenic right ventricular cardiomyopathy in plakoglobin-deficient mice. *J. Am. Coll. Cardiol.*, **57**, 740-750.

27.   Noorman M, Hakim S, Kessler E, Groeneweg JA, Cox MG, Asimaki A, van Rijen HV, van Stuijvenberg L, Chkourko H, van der Heyden MA, et al. (2013) Remodeling of the cardiac sodium channel, connexin43, and plakoglobin at the intercalated disk in patients with arrhythmogenic cardiomyopathy. *Heart Rhythm.*, **10**, 412-419.

24

28.   van Spaendonck-Zwarts KY, van den Berg MP, van Tintelen JP (2008) DNA analysis in inherited cardiomyopathies: current status and clinical relevance. *Pacing Clin. Electrophysiol.*, **31**, S46-49.

29.   Krishnamurthy S, Adhisivam B, Hamilton RM, Baskin B, Biswal N, Kumar M. (2011) Arrhythmogenic dilated cardiomyopathy due to a novel mutation in the desmoplakin gene. *Indian J., Pediatr.*, **78**, 866-869.

30.   van der Zwaag PA, van Rijsingen IA, Asimaki A, Jongbloed JD, van Veldhuisen DJ, Wiesfeld AC, Cox MG, van Lochem LT, de Boer RA, Hofstra RM, et al. (2012) Phospholamban R14del mutation in patients diagnosed with dilated cardiomyopathy or arrhythmogenic right ventricular cardiomyopathy: evidence supporting the concept of arrhythmogenic cardiomyopathy. *Eur. J. Heart Fail.*, **14**, 1199-1207.

31.   Garcia-Pavia P, Syrris P, Salas C, Evans A, Mirelis JG, Cobo-Marcos M, Vilches C, Bornstein B, Segovia J, Alonso-Pulpon L, et al. (2011) Desmosomal protein gene mutations in patients with idiopathic dilated cardiomyopathy undergoing cardiac transplantation: a clinicopathological study. *Heart.* **97**, 1744-1752.

32.   Cerrone M, Lin X, Zhang M, Agullo-Pascual E, Pfenniger A, Chkourko Gusky H, Novelli V, Kim C, Tirasawadichai T, Judge DP et al. (2014) Missense mutations in plakophilin-2 cause sodium current deficit and associate with a Brugada syndrome phenotype. *Circulation.*, **129**, 1092-1103.

33.   Peters S. (2014) Arrhythmogenic cardiomyopathy and provocable Brugada ECG in a patient caused by missense mutation in plakophilin-2. *Int. J. Cardiol.*, **173**, 317-318.

34.   van Hoorn F, Campian ME, Spijkerboer A, Blom MT, Planken RN, van Rossum AC, de Bakker JM, Wilde AA, Groenink M, Tan HL (2012) SCN5A mutations in Brugada syndrome are associated with increased cardiac dimensions and reduced contractility. *PLoS One.*, **7**, e42037.

Figure legends

Figure 1. **Generation of cardiac-specific transgenic mice lines expressing a truncated PKP2. A**) Scheme of construct designed containing α-MHC promoter upstream to truncated PKP2 (which only express the first 329 amino acids of the full protein), fused to tagged proteins T2a and Ruby. Auto-cleaved site is presented into T2a sequence as dashed line. **B**) Immunofluorescence analysis shows background signal in cardiac tissue of wild type (WT) heart (a-c). With the same intensity light than WT, Ruby auto-fluorescence (d), T2a immunolabeled (e) and merged images (f) are highlighted in the cardiac tissue of transgenic (TG) mice (line 4). An intense Ruby and T2a signal is observed at the ID. Bar=50μm. **C**) Relative transcript content of the transgene in liver and heart tissue of all 5 TG and WT lines. **D**) Cardiac transgenic protein expression in all 5 TG lines. **E**) Comparison of protein expression of truncated PKP2 in transgenic low-expression (TG-L; line 5 in D), transgenic medium-expression (TG-M; line 4 in D) and transgenic high-expression lines (TG-H; line 4+5).

Figure 2. **Truncated and native PKP2 localization and distribution in transgenic cardiomyocytes. A**) Native PKP2 (Green) is located at the ID of WT and transgenic lines. Truncated PKP2 (PKP2-T2a) is observed in the cytoplasm of cardiomyocytes (Red) and co-localized in the ID with native PKP2 (arrows). Also, a nuclear localization is observed in some transgenic cardiomyocytes (asterisks). Bar=20μm. **B**) Immunoblots of subcellular compartments proteins showing the distribution of PKP2-T2a in all compartments of the cell, whereas native PKP2 is only present in the membrane sub-fraction. All images are captured at the same time of exposition. Notice the great amount of both PKP2 versions in the cytoskeleton compartment. TG-M and WT mice of 7-months-old are used for both analyses.

27

Figure 3. **Intercalated disc defects in 10-months-old transgenic mice. A, B and C)** Low magnification of intercalated disc of WT, TG-M and TG-H cardiomyocytes, respectably. TG-H intercalated disc showed gaps between both membranes (arrows). **D, E and F)** High magnification of intercalated discs. TG-M showed normal intercalated disc aspect compared to WT (**D** and **E,** respectably). However, TG-H eventually showed completed rupture of intercalated discs (arrowhead in **F**). More detail in Supplementary Figure 4. The quantification of distance between cells at ID level showed significant increase of intercellular space (**G**). ***p<0.001. One-way ANOVA and Bonferroni post-test were used to comparison between groups.

Figure 4. Desmosome disassembly and adhesion reduction in 10-months-old TG-H mice. A, B and C) Low magnification of intercalated disc of WT, TG-M and TG-H cardiomyocytes, respectably. Notice the breakage of the ID in TG-H cardiomyocytes (arrow in **C**). The different layers of desmosomes were identified in the TG-M (**B1** and **2**), with similar electron density compared to WT (**A1** and **2**). Desmosomes showed a decrease of electron density in the different layers and reduction of contacts between both faces in TG-H hearts (arrowheads in **C1** and **2**).

Figure 5. **RVOT enlarges with transgene content, aging and exercise. A**) Representative short parasternal echocardiographic planes of 7 months-old mice showing the RVOT diameter (arrow). Ao=Aorta; Pl=Pulmonary artery; LA=Left Atria. **B**) Mean±SEM of RVOT diameter in adult (sedentary 7-months-old), old (12-months-old) and trained (Trained 7-months-old) groups. Note the increase of RVOT diameter correlated with transgene content in all groups. Exercise and aging increased the RVOT diameter in TG-L and TG-M. Number of animals per group is showed into each bar. *p<0.05; **p<0.01; ***p<0.001 vs WT within each group. †p<0.05 compared to the

same genotype from sedentary 7-months-old group. Two-way ANOVA and Bonferroni post-test were used to comparison between groups. More explanation in Table 1.

Figure 6. **Molecular disturbance of cellular adhesion proteins in transgenic mice. A and B**) Representative microphotographs of DSC2 and β-CAT localization in TG-M and TG-H cardiac tissue (Red). DES signal was used to define each cardiomyocyte (Green). **A**) DSC2 deposits were found in the cytoplasm of cardiomyocytes of TG-H (Arrows). **B**) The signal of β-CAT in the ID was reduced in TG-M and dramatically decreased in TG-H (Open arrows). The redistribution of β-CAT signal in the cytoplasm was evident in TG-H (asterisks). Bar=20μm. Low zoom images are showed in Supplementary Figure 6. **C**) Representatives blots of ventricular tissue lysates to different cellular adhesion proteins of ID. **D**) Relative amount of proteins to TG-M and TG-H (number of animals: WT=6; TG-M=4; TG-H=6). The protein level was normalized using GAPDH signal. All data show as mean±SEM. One-way ANOVA and Bonferroni post-test were used to comparison between groups. *p<0.05; **p<0.01 compared to WT group.

Figure 7. **Electrocardiogram abnormalities depend on transgene content but not on aging or exercise. A**) Example of surface ECG measurements to WT, TG-M and TG-H mice of 7 months of age. Slim bars indicate the PR interval. Thick bar=10ms. **B**) Mean values to PR interval (up) and QRS (down) duration to each group. Progressive PR interval prolongation is observed between genotypes. QRS is prolonged in TG-H of all groups. All data is showed as mean±SEM. *p<0.05; **p<0.01; ***p<0.001 compared to WT to each group; #p<0.05 compared to 7-months-old sedentary group. Two-way ANOVA and Bonferroni post-test were used to comparison between groups. More explanation in Supplementary Table.

Figure 8. Genetic- but not training-dependent arrhythmias induction in truncated PKP2 transgenic mice. **A**) Representative ventricular taquiarrhythmia (VT) induction after burst pacing (stimuli) showed in surface (ECG; red line) and intracavitary electrogram (EGM; blue line) in a sedentary TG-H mouse. Bar=100ms. **D**) Percentage of animals with induced ventricular arrhythmias in sedentary and trained groups of 7-months-old. VTs occur more often in transgenic sedentary groups compared to WT. No differences were observed in trained groups. Mantel-Haenszel linear-by-linear Association was performed to test the linear relationship between groups, establishing the dependence between transgene dose and arrhythmia inducibility. More explanation in Table 2.

Figure 9. **Remodeling and reduction of CX43 and Na$_v$1.5 channels in transgenic hearts.** **A**) CX43 remodeling is observed in the ID of TG-H cardiomyocytes (arrow). Not evident remodeling is observed in TG-M cardiomyocytes. **B**) Reduction of Na$_v$1.5 signal in ID of TG-M is detected. More decreased of its signal is detected in TG-H (arrows). **B**) Significant reduction of CX43 protein content in TG-M and TG-H cardiac tissue. **C**) Significant reduction of Na$_v$1.5 protein content in TG-H hearts. *$p<0.05$; ***$p<0.001$ compared to WT. One-way ANOVA or Kruskal-Wallis were used to comparison between groups, and respective Bonferroni or Dunnet post-test were used to pairwise comparison. Number of animals to each protein: WT=6; TG-M=4; TG-H=6. Low zoom images of both proteins are showed in Supplementary Figure 7.

30

	7 Months (24-32 Weeks)				12 Months (48-56 Weeks)				7 Months Trained (24-32 Weeks)		
	WT	TG-L	TG-M	TG-H	WT	TG-L	TG-M	TG-H	WT	TG-L	TG-M
n (♂/♀)	16 (10/6)	9 (4/5)	12 (6/6)	9 (4/5)	10 (3/7)	5 (2/3)	5 (1/4)	8 (4/4)	8 (4/4)	9 (4/5)	10 (5/5)
IVS (mm)	0.69±0.01	0.65±0.02	0.73±0.01	0.69±0.02	0.63±0.02	0.66±0.02	0.67±0.03	0.71±0.01	0.66±0.02	0.64±0.02	0.76±0.01
PW (mm)	0.7±0.01	0.65±0.02	0.74±0.01	0.68±0.01	0.65±0.02	0.68±0.02	0.65±0.03	0.72±0.01	0.67±0.03	0.66±0.02	0.76±0.01
LVEDD (mm)	4.03±0.05	3.73±0.09	3.98±0.07	4.09±0.09	4.03±0.09	4.12±0.12	4.15±0.12	4.34±0.08	4.04±0.11	4.13±0.09	4.07±0.04
LVESD (mm)	2.8±0.09	2.63±0.14	2.76±0.08	3.16±0.12	2.84±0.11	3.05±0.14	2.65±0.12	3.22±0.91	2.91±0.19	3.04±0.08	2.91±0.06
LVFS (%)	30.7±1.9	31.7±2.4	30.7±1.3	22.9±2.5*	29.7±1.8	26.2±1.7	29±1.9	25.9±0.9*	28.3±3.2	26.3±1.3	28.3±1.4
LV mass (mg)	98.1±3.22	83.6±4.9	103.4±4.3	98.2±4.1	89.2±6.4	97.1±7.5	95.3±5.8	115.9±6†	93.6±6.5	93.7±6.6	111.7±2.7
RVOT (mm)	2.11±0.04	1.99±0.02	2.27±0.06	2.49±0.07‡	2±0.05	2.32±0.07†	2.45±0.1‡	2.5±0.05‡	2.08±0.02	2.27±0.06	2.47±0.08‡
RVAD (mm^2)	3.85±0.15	4.2±0.2†	4.2±0.1*	5.03±0.14‡	4.17±0.2	5.29±0.16†	5.2±0.32*	5.7±0.22‡	3.98±0.16	5.3±0.31†	5±0.2†
TAPSE (mm)	1.06±0.02	1.03±0.02	0.94±0.03	0.86±0.02‡	1.07±0.01	0.87±0.07‡	0.94±0.03*	0.78±0.03‡	1.01±0.01	0.97±0.07	1.02±0.02

31

TP/ET	0.26±0.01	0.28±0.01	0.29±0.01	0.34±0.01‡	0.27± 0.01	0.29± 0.01	0.3± 0.01	0.31± 0.01‡	0.29±0.02	0.3± 0.01	0.31±0.01

Table 1: Echocardiographic measurements in all groups.

IVS=interventricular septum thickness; PW= LV Posterior Wall Thickness; LVEDD= LV end-diastolic diameter; LVESD= LV end-systolic diameter; LVFS= LV fraction shortening; RVAD= RV end-diastolic area parasternal axis view; RVOT= RV outflow tract; Acc= myocardial acceleration during isovolumic contraction; TAPSE= tricuspid annular plane systolic excursion. TP/ET= time to pulmonary pressure peak to RV ejection time ratio. *$p<0.05$; †$p<0.01$; ‡<0.001 compared with WT to each group. 2-way measures ANOVA and Bonferroni post-test to pairwise comparison were performed.

32

	Sedentary				Trained			p value (Genotype)	p value (Exercise)
	WT (n=13)	TG-L (n=7)	TG-M (n=13)	TG-H (n=23)	WT (n=8)	TG-L (n=6)	TG-M (n=9)		
A-H Interval (ms)	22.6±0.8	24.8±2.4	25.6±1.3*	27.1±1.2[‡]	20.7±0.8	25.9±1.7	22.9±0.7*	0.006	0.570

33

H-V Interval (ms)	10.9±0.6	12.67±0.6	13.3±1.1	10±0.4	11.2±0.5	11.6±1	11.8±1.1	0.044	0.459
VERP (ms)	40.2±1.1	40.2±1.1	41.3±1.3	42±0.8*	37.4±1.6	45.2±1.7	40.5±1.2	INT	INT
VT-induced	4/13(31%)	4/7(57%)	7/13(54%)	17/23(74%)	4/8(50%)	3/6(50%)	5/9(56%)	p=0.01 (for trend in sedentary)	

Table 2. Results for electrophysiological studies in 7-month-old mice.

VERP= ventricular effective refractory period; VT= ventricular tachycardia. *$p < 0.05$; [‡]$p < 0.001$ compared with WT to each group. Two-way-ANOVA and Bonferroni post-test to multiple comparisons were performed in continuous variables. INT= main-factors interaction. Mantel-Haenszel linear-by-linear Association was performed to test the trend in categorical variable.

Abbreviations

ACM: Arrhythmogenic cardiomyopathy

PKP2: Plakophilin-2

DSP: Desmoplakin

PG: Plakoglobin

DES: Desmin

DSC2: Desmocollin-2

DSG2: Desmoglein-2

CX43: Connexin-43

$Na_v1.5$: α-subunit of cardiac sodium channel

TG-L: Transgenic mouse with low expression

TG-M: Transgenic mouse with medium expression

TG-H: Transgenic mouse with high expression

β-CAT: beta-Catenin

α-MHC: alpha-Myosin Heavy Chain

PCR: Polymerase chain reaction

ECG: Electrocardiogram

VT: Ventricular tachycardia

EGM: Electrogram

TAPSE: Tricuspid annular plane systolic excursion

LVFS: Left ventricle fraction shortening

ID: Intercalated disc

GAPDH: Glyceraldehide-3-phosphate dehydrogenase

H3K9: Histone H3 tri-methyl K9

WT: Wild type

RVOT: Right ventricle outflow tract

DCM: Dilated cardiomyopathy

BrS: Brugada Syndrome
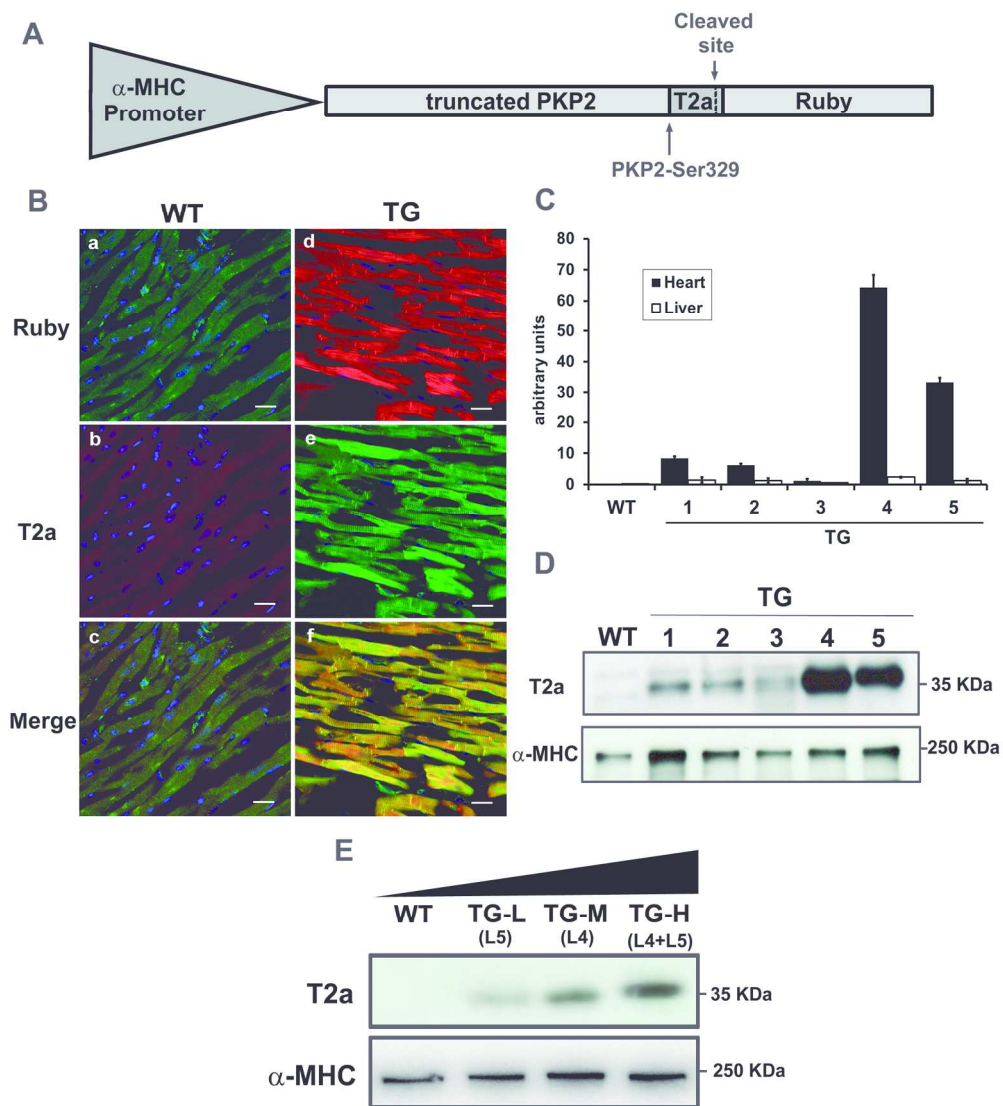
Generation of cardiac-specific transgenic mice lines expressing a truncated PKP2
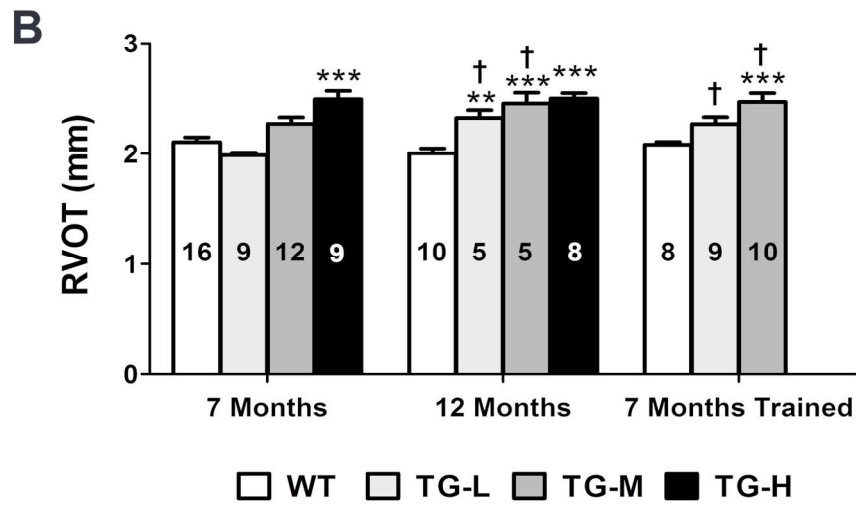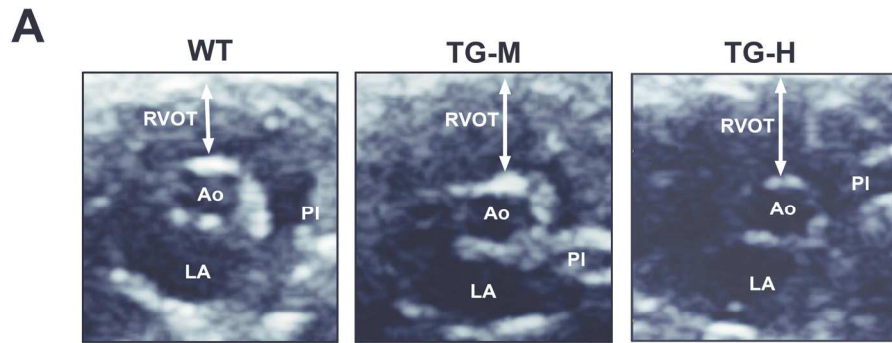180x199mm (300 x 300 DPI)
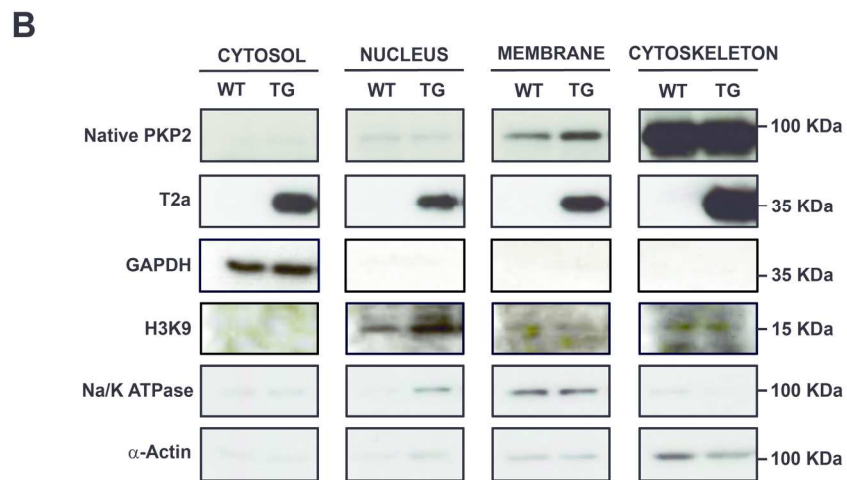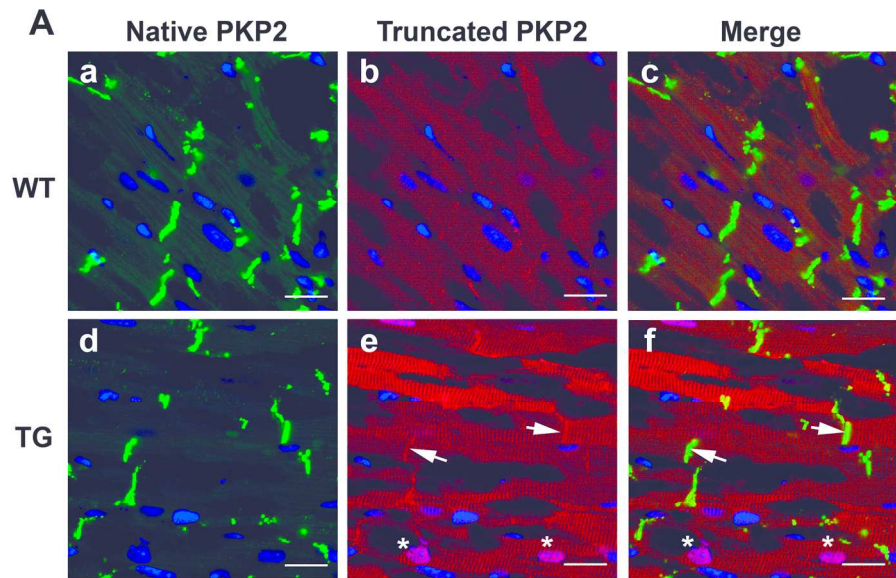
Truncated and native PKP2 localization and distribution in transgenic cardiomyocytes
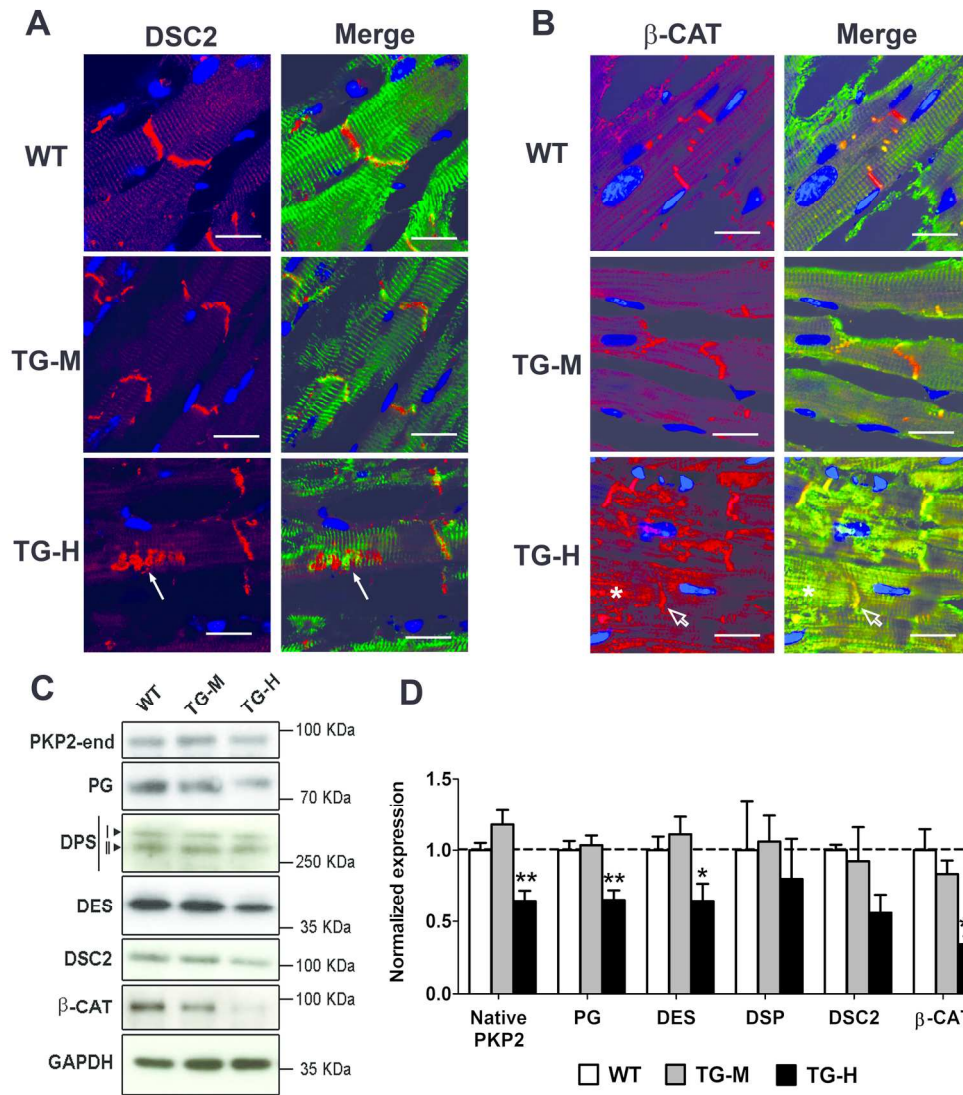180x199mm (300 x 300 DPI)

WT   TG-M   TG-H
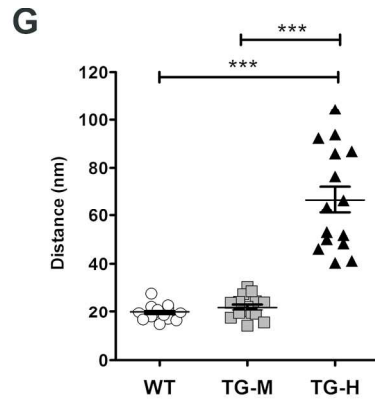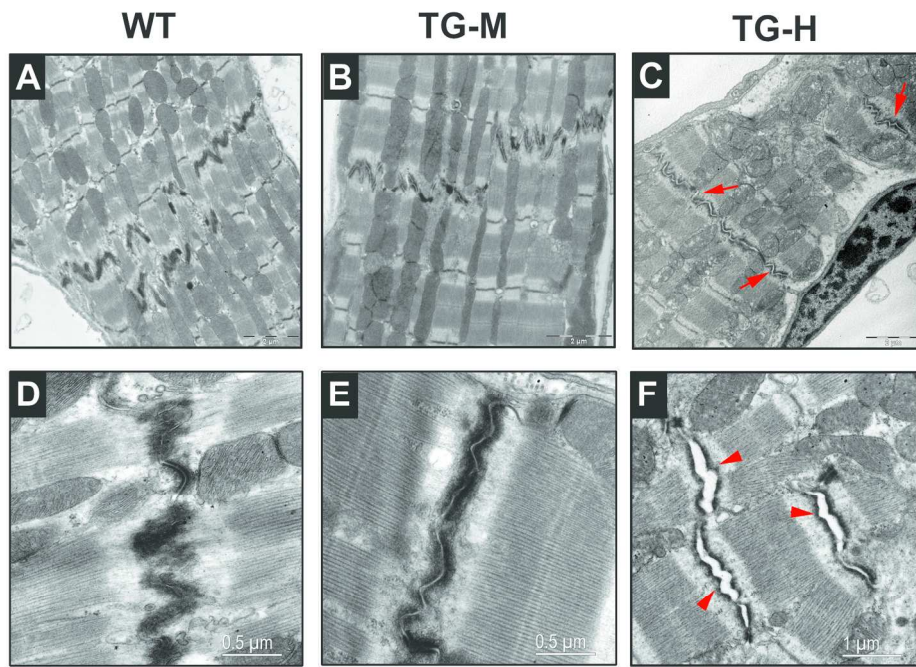
Intercalated disc defects in 10-months-old transgenic mice
180x199mm (300 x 300 DPI)
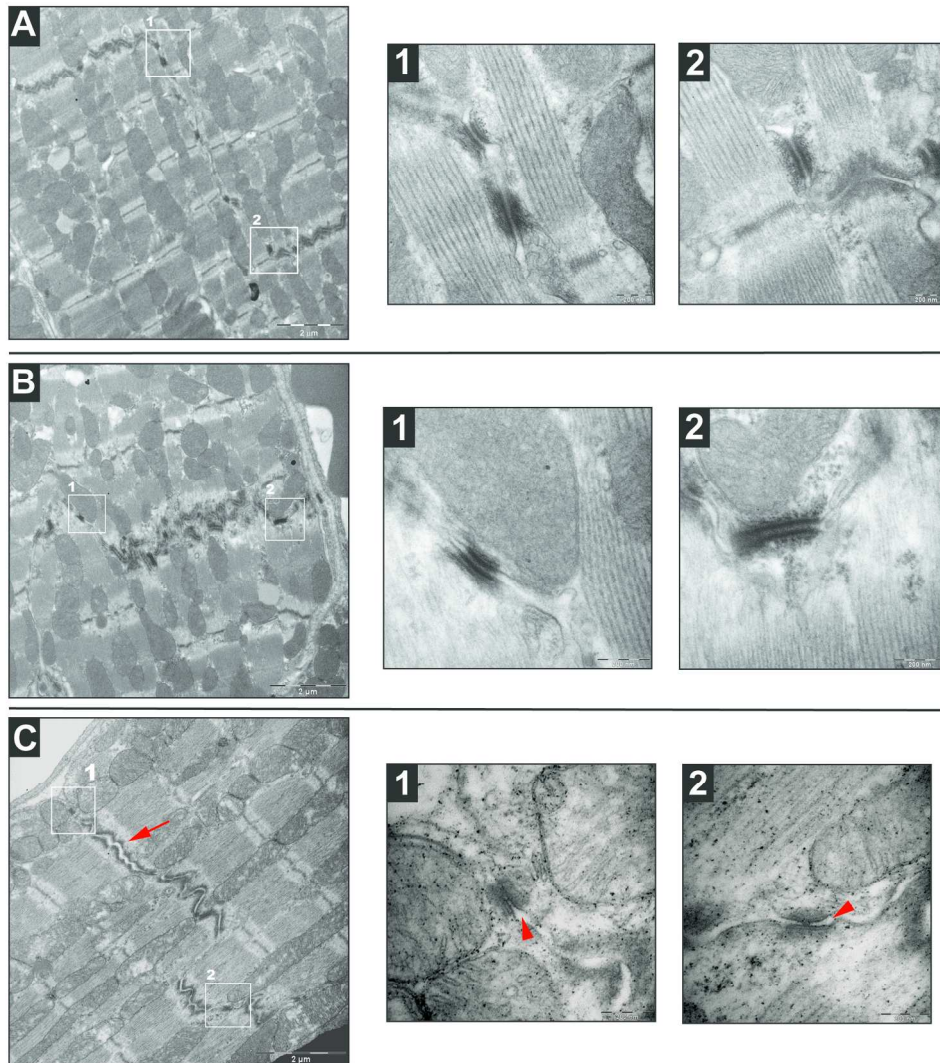
Desmosome disassembly and adhesion reduction in 10-months-old TG-H mice
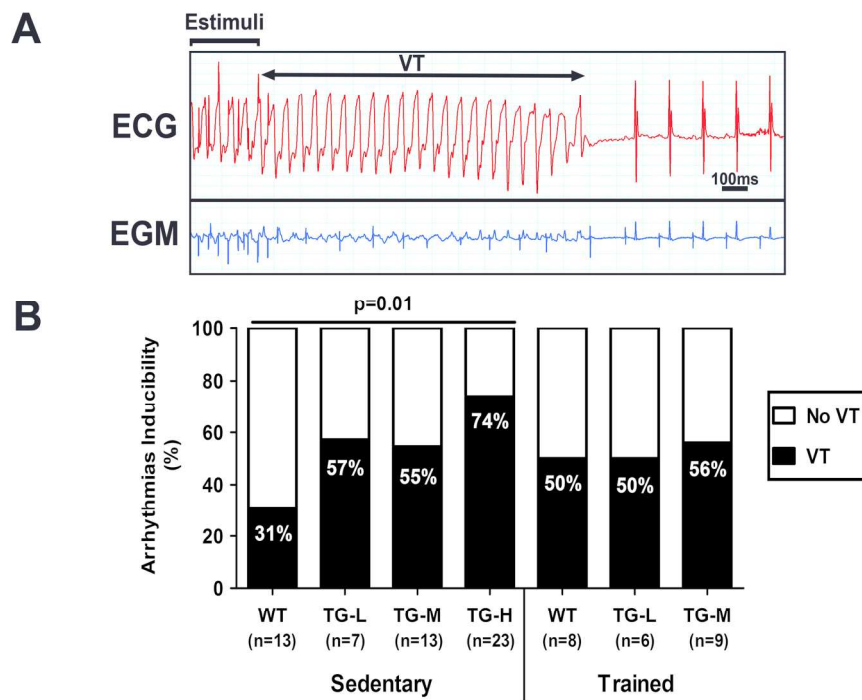180x199mm (300 x 300 DPI)

A

WT   TG-M   TG-H

B

RVOT enlarges with transgene content, aging and exercise
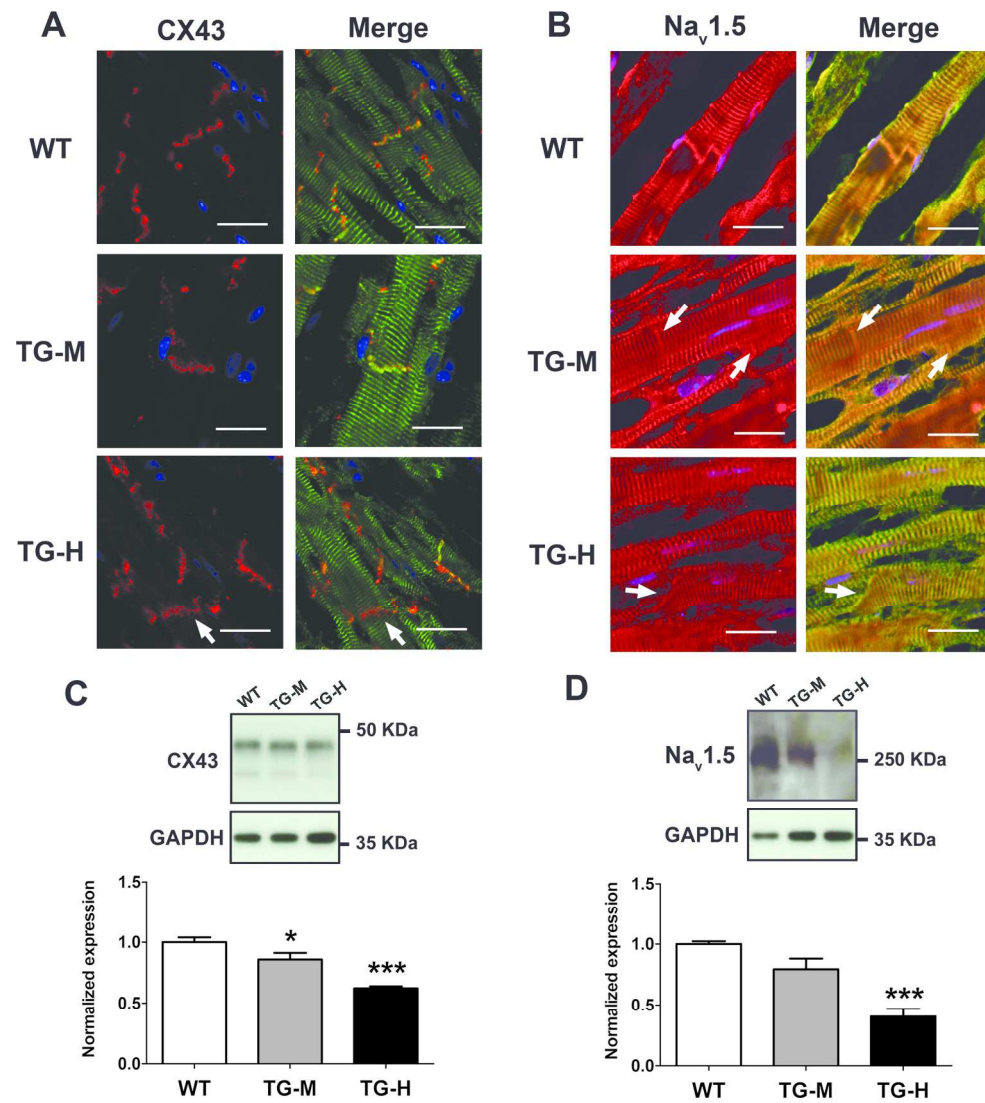180x170mm (300 x 300 DPI)

Molecular disturbance of cellular adhesion proteins in transgenic mice
180x199mm (300 x 300 DPI)
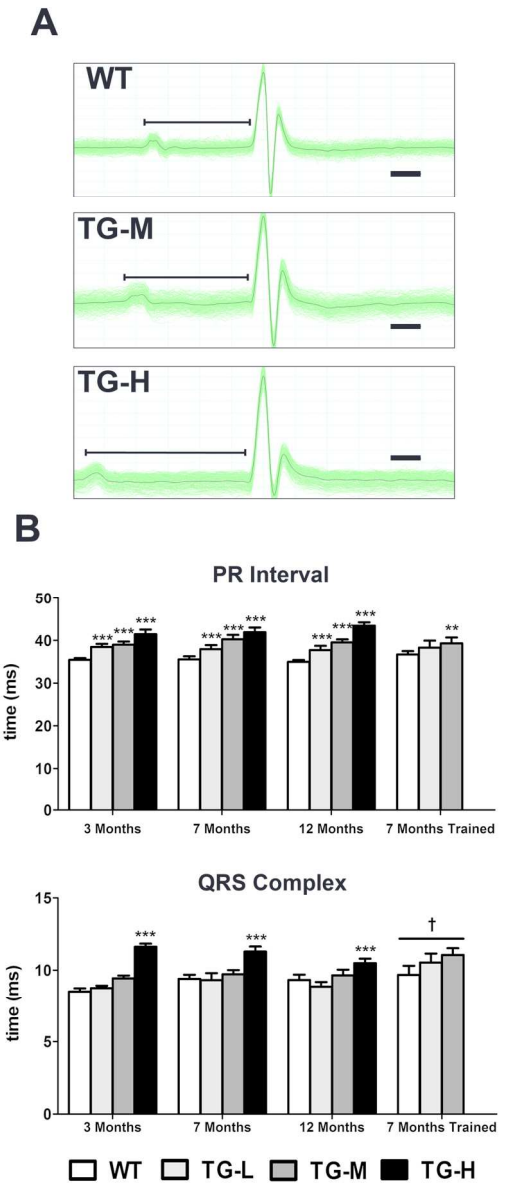
Electrocardiogram abnormalities depend on transgene content but not on aging or exercise
86x199mm (300 x 300 DPI)

A

Estimuli

VT

ECG

100ms

EGM

B

p=0.01

No VT
VT

31%

57%

55%

74%

50%

50%

56%

Arrhythmias Inducibility (%)

WT
(n=13)

TG-L
(n=7)

TG-M
(n=13)

TG-H
(n=23)

WT
(n=8)

TG-L
(n=6)

TG-M
(n=9)

Sedentary

Trained

Genetic- but not training-dependent arrhythmias induction in truncated PKP2 transgenic mice
180x129mm (300 x 300 DPI)

Remodeling and reduction of CX43 and Nav1.5 channels in transgenic hearts
180x199mm (300 x 300 DPI)